














**Evidence of the effect of strong stripping channels on the dynamics of the  $^8\text{Li} + ^{58}\text{Ni}$  reaction**

O. C. B. Santos <sup>\*</sup>, R. Lichtenthaler <sup>†</sup>, K. C. C. Pires , U. Umbelino , E. O. N. Zevallos , A. L. de Lara ,  
A. S. Serra , V. Scarduelli , J. Alcantara-Nunez , V. Guimaraes , A. Lepine-Szily , and J. C. Zamora   
*Departamento de Fısica Nuclear, Instituto de Fısica, Universidade de Sao Paulo, 05508-090 Sao Paulo, Brazil*

A. M. Moro 

*Departamento de Fısica Atomica, Molecular y Nuclear, Facultad de Fısica, Universidad de Sevilla, Apartado 1065, E-41080 Sevilla, Spain  
and Instituto Interuniversitario Carlos I de Fısica Teorica y Computacional (iCI), Apartado 1065, E-41080 Sevilla, Spain*

S. Appannababu 

*Department of Nuclear Physics, Andhra University, Visakhapatnam 530 003, India*

M. Assuncao 

*Departamento de Fısica, Universidade Federal de Sao Paulo, UNIFESP, 09913-030 Diadema, Brazil*

A. Barioni 

*Departamento de Ciencias do Mar, Universidade Federal de Sao Paulo, UNIFESP, 11070-100 Sao Paulo, Brazil*

R. Linares , V. A. B. Zagatto , and P. N. de Faria 


*Departamento de Fısica, Universidade Federal Fluminense do Rio de Janeiro, 24210-340 Rio de Janeiro, Brazil*

M. C. Morais 

*INFES, Universidade Federal Fluminense, Santo Antonio de Padua, 28470-000 Rio de Janeiro, Brazil*

V. Morcelle 

*Universidade Federal Rural do Rio de Janeiro, Seropedica, 23890-000 Rio de Janeiro, Brazil*

J. M. B. Shorto 

*Instituto de Pesquisas Energeticas e Nucleares, IPEN-CNEN/SP, 05508-000 Sao Paulo, Brazil*

Jin Lei 

*Istituto Nazionale di Fisica Nucleare, Sezione di Pisa, Largo Pontecorvo 3, 56127 Pisa, Italy*



(Received 30 December 2020; revised 4 March 2021; accepted 6 May 2021; published 1 June 2021)

The  $^8\text{Li} + ^{58}\text{Ni}$  collision is investigated at 23.9, 26.1, 28.7, and 30 MeV bombarding energies. Quasielastic angular distributions and the singles  $^7\text{Li}$  angular and energy distributions are presented. Coupled-reaction channels (CRC) calculations, which include the coupling of the elastic channel to  $^{59}\text{Ni} = ^{58}\text{Ni} + n$  states above and below the neutron threshold, provide a simultaneous description of the quasielastic and transfer distributions and evidence the strong effect of the one-neutron transfer/breakup channels on the quasielastic scattering. The  $^7\text{Li}$  angular and energy distributions have been also successfully analyzed combining the continuum discretized coupled channels (CDCC) method, for the elastic breakup, and the IAV model of Ichimura, Austern, and Vincent [Phys. Rev. C **32**, 431 (1985)], for the nonelastic breakup. These calculations indicate that most of the  $^7\text{Li}$  yields are due to nonelastic breakup contributions (transfer), whereas elastic breakup plays a minor role.

DOI: [10.1103/PhysRevC.103.064601](https://doi.org/10.1103/PhysRevC.103.064601)

**I. INTRODUCTION**

Experiments with nuclei outside the valley of stability have been performed in several laboratories all over the world in

recent decades. Interesting new phenomena have been observed related to the structure of the so-called exotic nuclei, in particular, in the light mass region where features such as cluster structure and neutron/proton halos are present. Clustering is a common property of light nuclei, such as helium, lithium, beryllium, and boron isotopes, and stems from their low binding energies and large spectroscopic factors for certain configurations [1]. In particular, the lithium

<sup>\*</sup>osvaldo.santos@usp.br

<sup>†</sup>rubens@if.usp.br

isotope chain has five known bound isotopes:  ${}^{6-9,11}\text{Li}$ .  ${}^{6,7}\text{Li}$  are stable with separation energies of 1.47 and 2.47 MeV to break up into  $\alpha + d$  and  $\alpha + t$  respectively, with ground state spectroscopic factors ranging from 0.85 to 1. Such small binding energies contrast with the separation energies for stable nuclei, which are in the range of 7–10 MeV.  ${}^{11}\text{Li}$  is a very exotic nucleus with a pronounced neutron halo [2–4] formed by the two valence neutrons weakly bound to the  ${}^9\text{Li}$  core;  $S_{2n} = 0.369$  MeV. In addition to its low separation energy, the low angular momenta of the valence neutrons make their wave functions extend to large distances from the nuclear core, forming a nuclear halo.  ${}^6\text{He}$  ( $S_{2n} = 0.973$  MeV) and  ${}^8\text{B}$  ( $S_p = 0.138$  MeV) are other examples of exotic nuclei in this mass region which present neutron and proton halos, respectively. Although weakly bound,  ${}^8\text{Li}$  is not so exotic, with a separation energy of 2.03 MeV to dissociate into  $n + {}^7\text{Li}$  [5–13].

Due to the projectile's low binding energy and cluster structure, many reaction channels are open in the collisions between these near drip-line nuclei and stable target nuclei. At intermediate and high bombarding energies (from 20 MeV/nucleon up to 1 GeV/nucleon) projectile breakup appears as a dominant reaction mechanism and there is a vast amount of literature emphasizing the importance of breakup reactions in collisions induced by exotic nuclei [2–4,14].

In the low-energy domain ( $\leq 10$  MeV/nucleon), the projectile cluster and halo structure manifests as an enhancement in the total reaction cross section and a strong coupling between different reaction channels [15–24]. The identification of the reaction channels that effectively contribute to the total reaction cross section enhancement is still a challenge for both theory and experiment. For stable nuclei, fusion is the most important nonelastic process in terms of cross section, followed by inelastic scattering and particle transfer channels to bound states with lower cross sections. In the case of weakly bound exotic projectiles, breakup (noncapture breakup, incomplete fusion, etc.) and transfer channels are usually highly populated and may have cross sections comparable to fusion [16,25]. Experimental evidences indicate that these reactions populate mainly highly excited states below and above the particle emission thresholds of the recoil nucleus [16,25–29], and may strongly affect the elastic scattering and fusion cross sections via coupling channel effects. In this complex coupled channels picture, new experimental data seems to be of paramount importance to identify the dominant channels in each particular case.

The importance of nuclei out of the valley of stability extends beyond the nuclear physics realm and may have consequences also in astrophysics. The synthesis of elements heavier than iron is one of the fundamental questions in nowadays cosmology. Nucleosynthesis proceeds through a series of capture reactions beginning in the light mass region and extending all the way up to the synthesis of heavier nuclei, and the importance of  $A = 5, 8$  masses is notably relevant [30–32]. There are no stable nuclei of masses 5 and 8 and these gaps act as barriers to the synthesis of heavier elements. As a consequence, the presence of such nuclei in explosive scenarios could provide ways to overcome this barrier.

In this paper we present new experimental data of reactions induced by the radioactive  ${}^8\text{Li}$  nucleus on a  ${}^{58}\text{Ni}$  target at four incident energies above the Coulomb barrier. A preliminary analysis of one of the angular distributions presented in this work has been published in Ref. [33]. Although similar systems have been investigated previously [11,12], here we present a more complete set of quasielastic scattering and neutron stripping angular distributions, covering an angular region from forward to backward angles around the grazing angle, where an enhancement of the quasielastic cross section with respect to the bare optical potential is clearly observed in the experimental data.

The quasielastic scattering and the  ${}^7\text{Li}$  production channels have been analyzed and compared with several theoretical models. The paper is organized as follows. In Sec. II the experimental setup and the experimental data are presented. In Sec. III we discuss the theory and present the analysis results. In Sec. IV we draw our conclusions.

## II. EXPERIMENTAL SETUP

The experiment was performed in the RIBRAS (Radioactive Ion Beams in Brasil) facility at the Nuclear Physics Open Laboratory (LAFN, acronym in portuguese) of the University of Sao Paulo [34–37]. The  ${}^7\text{Li}$  primary beam was delivered by the 8-UD Pelletron accelerator with 26–32 MeV energy and 200 e nA impinging in the RIBRAS primary scattering chamber where a  $12 \mu\text{m}$   ${}^9\text{Be}$  foil was used as production target. The  ${}^8\text{Li}$  beam was produced by the  ${}^9\text{Be}({}^7\text{Li}, {}^8\text{Li})$  reaction.

The secondary  ${}^8\text{Li}$  particles are collected within the first solenoid angular acceptance ( $2^\circ \leq \theta \leq 6^\circ$ ), selected, and focused on the scattering chamber where a  $4.5 \text{ mg/cm}^2$  gold foil was placed to scatter the  ${}^8\text{Li}$  particles and monitor the secondary beam intensity. The solenoid current was previously estimated, at each energy, using the TWSP code [38] for the  ${}^8\text{Li}$  trajectories along the solenoid all the way up to the secondary target and was varied around the calculated values in order to experimentally maximize the  ${}^8\text{Li}_{\text{g.s.}}$  beam intensity in the secondary target position. The  ${}^8\text{Li}$  secondary beam intensity was of about  $10^5$  pps during the experiment. A 99.997% isotopically enriched,  $2.1 \text{ mg/cm}^2$   ${}^{58}\text{Ni}$  foil was used as secondary target.

Four  $\Delta E(25\text{--}50 \mu\text{m})\text{-}E(1000 \mu\text{m})$ ,  $150 \text{ mm}^2$  area silicon telescopes were mounted in the rotating plate to detect and identify the scattered particles. The geometrical detection solid angles were of about 20.7 msr with an angular acceptance of approximately  $\pm 4.0^\circ$ . A “nose” with two sets of collimators was installed in front of the telescopes to ensure that all particles reaching the detectors were indeed coming from the secondary target.

Two-dimensional  $\Delta E\text{-}E$  spectra obtained with  ${}^{58}\text{Ni}$  and gold targets are presented in Fig. 1. In Fig. 1(b) we basically see the secondary beam composition. The elastically scattered  ${}^8\text{Li}$  particles are well separated from the  $\alpha$  particles and other contaminants such as  ${}^6\text{He}$ ,  $p$ ,  $d$ ,  $t$ . The  ${}^8\text{Li}$  secondary beam is produced in the ground state (g.s.) and in its first excited state (0.98 MeV,  $1^+$ ) with 8.2 fs half-life. In Fig. 2 we show a projection on the energy axis of the two  ${}^8\text{Li}$  peaks from

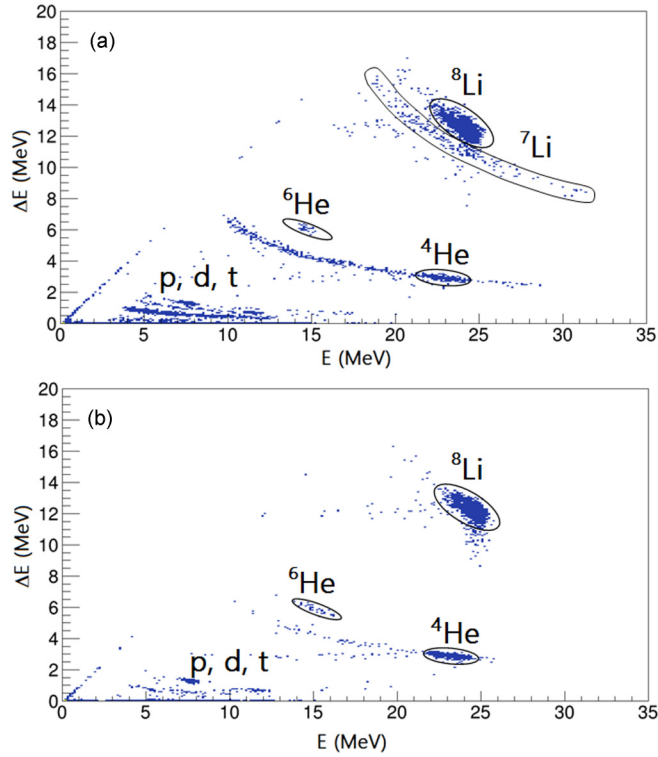


FIG. 1. Two-dimensional  $\Delta E$ - $E$  spectra obtained with (a)  $^{58}\text{Ni}$  and (b) gold targets at  $\theta_{\text{lab}} = 35^\circ$  and incident energy of 26.1 MeV [37].

Figs. 1(a) and 1(b). With the gold target (b) it is possible to separate two  $^8\text{Li}$  elastic peaks but with the nickel target (a) at the backwards angles region it becomes very difficult to separate these two peaks. For this reason we decided to include both in the total  $^8\text{Li}$  peak area to calculate the cross sections in a consistent way. It is important to mention that the lower energy peak seen in Fig. 2 includes both low energy events coming from the primary target and possible events from the  $^8\text{Li}(1^+; 0.98)$  excitation in the secondary target. However, the events from the  $^8\text{Li}$  excitation are of minor importance, as will be demonstrated in the next section.

The  $^7\text{Li}$  events observed below the elastic  $^8\text{Li}$  peak in Fig. 1(a) are not present in the gold target spectrum, indicating that  $^7\text{Li}$  particles are not beam contaminants but are being produced in reactions with the  $^{58}\text{Ni}$  target. The  $^7\text{Li}$  line presents a wide energy distribution concentrated mainly below the elastic peak but extending also to higher energies. This energy distribution corresponds to the population of different excited states in the final ( $^{59}\text{Ni}$ ) nucleus, corresponding to different  $^{58}\text{Ni}(^8\text{Li}, ^7\text{Li})$  reaction  $Q$  values from its ground state ( $Q_{\text{g.s.}} = 7$  MeV) up to higher excitation energies around and above 7 MeV ( $Q \leq 0$ ). At this point, we cannot decide whether these  $^7\text{Li}$  particles are coming from the neutron transfer or the  $^8\text{Li}$  breakup, as we will discuss in more detail further.

The secondary beam intensity was monitored during the experiment by performing gold target runs before and after every  $^{58}\text{Ni}$  run. The cross sections were determined from the

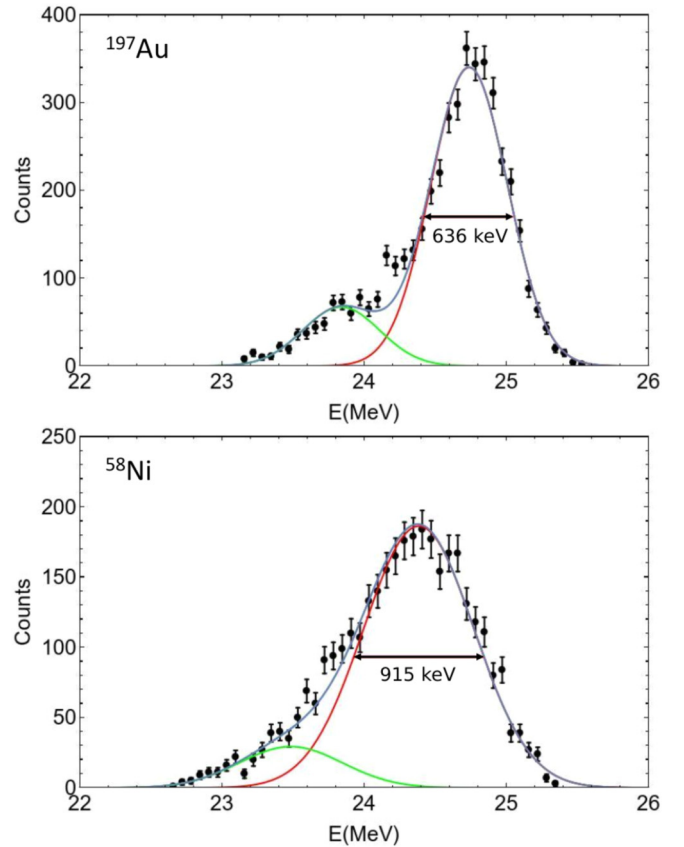


FIG. 2. Projection of the  $^8\text{Li}$  peaks from Fig. 1 on the total energy axis. FWHMs for gold and nickel targets are shown in the figure. The solid lines are Gaussian fits.

expression

$$\sigma_{\text{cm}}^{\text{Ni}}(\theta) = \frac{N_{\text{Ni}}^{\text{c}} N_{\text{Au}}^{\text{b}} N_{\text{Au}}^{\text{t}} J^{\text{Ni}}}{N_{\text{Au}}^{\text{c}} N_{\text{Ni}}^{\text{b}} N_{\text{Ni}}^{\text{t}} J^{\text{Au}}} \sigma_{\text{cm}}^{\text{Au}}(\theta), \quad (1)$$

where  $N^{\text{c}}$  is the number of counts in the peak of interest,  $N^{\text{b}}$  is the total number of incident  $^8\text{Li}$  beam particles during the run,  $J$  is the Jacobian factor which transforms from the laboratory to the center-of-mass system,  $N^{\text{t}}$  is the areal density of the target in number of atoms/cm<sup>2</sup>, and  $\sigma_{\text{cm}}^{\text{Au}}(\theta)$  is the  $^8\text{Li} + ^{197}\text{Au}$  Rutherford cross section. We take the ratio  $N_{\text{Au}}^{\text{b}}/N_{\text{Ni}}^{\text{b}}$  as being equal to the ratio between the primary beam integrated currents in each run. Here we suppose that the  $^8\text{Li}$  production rate is constant in both the gold target and the adjacent Ni target runs. The advantage of this method is that it is independent of the detectors solid angles.

The  $^8\text{Li} + ^{58}\text{Ni}$  elastic scattering and  $^7\text{Li}$  angular distributions, measured at 23.9, 26.1, 28.7, and 30 MeV, are shown in Figs. 3 and 4. These energies are well above the Coulomb barrier  $V_{\text{CB}}^{\text{(lab)}} = 13.55$  MeV for this system [39].

The errors have been calculated considering two components: the statistical errors on the ratio  $N_{\text{Ni}}^{\text{c}}/N_{\text{Au}}^{\text{c}}$  in Eq. (1) and an additional term  $\lambda$  which was obtained from the fluctuation in the  $\sigma/\sigma_{\text{Ruth}}$  ratio measured with the gold target at forward angles. This fluctuation around  $\sigma/\sigma_{\text{Ruth}} \approx 1$  was estimated to be of the order of 6% and was included in all data from

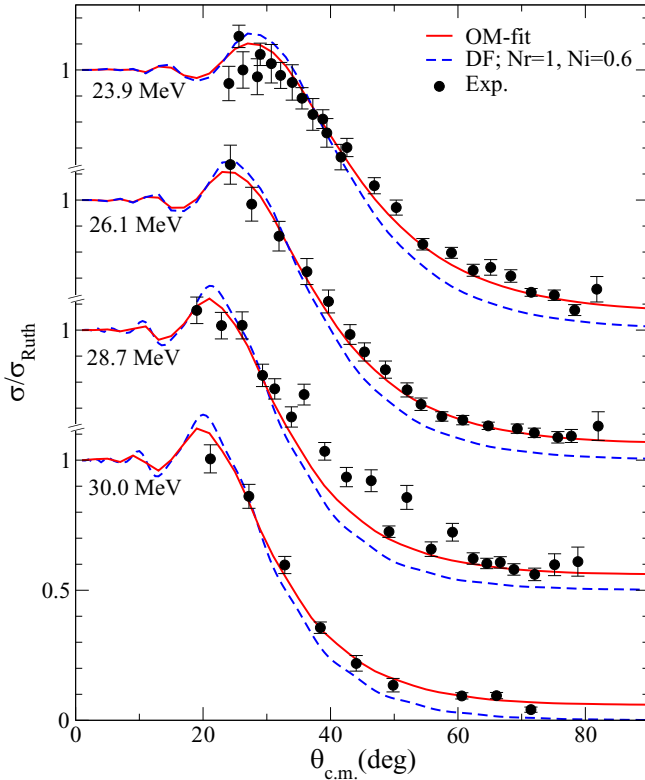


FIG. 3. The  ${}^8\text{Li} + {}^{58}\text{Ni}$  elastic scattering angular distributions relative to Rutherford compared with optical model fits obtained with a double-folding potential (with scaling factors  $N_r = 1$  and  $N_i = 0.6$ ) supplemented with a derivative Woods-Saxon potential (solid lines). The dashed lines are optical model calculations obtained with the double-folding potential alone.

forward to backward angles, being more relevant only at forward angles where the statistical errors are smaller.

The  ${}^7\text{Li}$  production cross sections (Figs. 4 and 5) were obtained by integrating the yields along the  ${}^7\text{Li}$  line shown in the  $\Delta E$ - $E$  spectrum. In Fig. 5, we show the  ${}^7\text{Li}$  energy spectra as a function of the  ${}^{58}\text{Ni}({}^8\text{Li}, {}^7\text{Li}) {}^{59}\text{Ni}$  reaction  $Q$  value. To obtain this distribution, the  $E_{7\text{Li}}$  axis was transformed to  $Q = Q_{\text{g.s.}} - E_x$  where  $Q_{\text{g.s.}} = 7.0$  MeV is the gs reaction  $Q$  value of the transfer reaction and  $E_x$  is the excitation energy of the recoil nucleus. The latter is obtained from the measured  $E_{7\text{Li}}$  using the analytical expression for the kinematics of the transfer reaction. The advantage of this procedure is that the  $Q$  value distribution does not depend on the scattering angle, whereas  $E_{7\text{Li}}$  does, allowing the summation of the  ${}^7\text{Li}$  yields measured at different angles. The upper horizontal axis in Fig. 5 stands for the excitation energy of the recoil nucleus  ${}^{59}\text{Ni}$ . The obtained  ${}^7\text{Li}$  energy distributions are consistent to what is expected from  $Q$ -optimum considerations for a neutron transfer reaction [40].

### III. THEORETICAL ANALYSIS

#### A. Optical model and coupled channels (CC) calculations

The measured quasielastic differential cross sections were first compared with optical model calculations. The real part

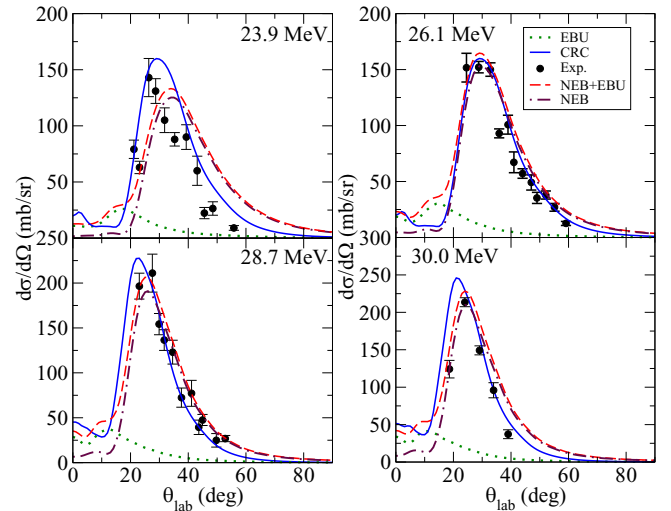


FIG. 4.  ${}^7\text{Li}$  angular distributions compared with CRC (solid lines), CDCC (dotted), and IAV (dashed-dotted) calculations. Dashed lines are the sum of the CDCC and IAV. See text for more details.

of the  ${}^8\text{Li} + {}^{58}\text{Ni}$  potential was generated by a double-folding (DF) procedure, convoluting the M3Y nucleon-nucleon interaction with the  ${}^8\text{Li}$  ground-state density from the microscopic calculation of Descouvemont *et al.* [41] and the  ${}^{58}\text{Ni}$  ground-state density obtained from a Hartree-Fock calculation with the Skyrme SkX interaction [42]. For the Coulomb potential, we considered that of a uniformly charged sphere of radius  $R_c = 1.25 \times (8^{1/3} + 58^{1/3})$  fm. For the imaginary part, we first attempted to use the same geometry as the real part, multiplied by some scaling factor ( $N_i$ ). This procedure, however, did not provide reasonable fits of the data, unless unusually large values of  $N_i$  were adopted ( $N_i > 1$ ). For more standard

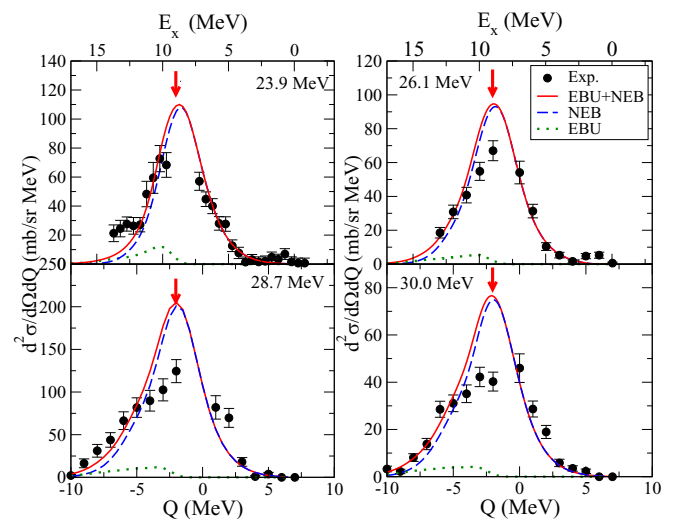


FIG. 5. Experimental  $Q$ -value distribution derived from the measured  ${}^7\text{Li}$  energy distributions compared with CDCC (dotted) and IAV (dashed) calculations. Solid lines are the sum of the IAV and CDCC. The arrows separates the unbound (left) from bound (right) states in  ${}^{59}\text{Ni}$ . See text for details.

values ( $N_i \approx 0.6-0.8$ ), the calculation does not reproduce well the measured distribution, as illustrated in Fig. 3 (dashed line) for the choice  $N_i = 0.6$ . The DF calculation (dashed line) clearly overestimates the cross sections at forward angles, around the Fresnel peak, and underestimates at intermediate angles.

An effect that could contribute for the observed intermediate angle rise of the cross sections would be a contamination, in the elastic peak, of events coming from the  ${}^8\text{Li}(0.98; 1^+)$  inelastic excitation, as discussed in Sec. II. To estimate this effect we performed CC calculations, including the coupling to the first ( $1^+$ ; 980 keV) and second ( $3^+$ ; 2.26 MeV) excited states of  ${}^8\text{Li}$ . Coulomb and nuclear excitation contributions were considered in the calculations, assuming the experimental value of the Coulomb excitation probability  $B(E2) = 55 e^2\text{fm}^4$  measured in Ref. [43] and a nuclear deformation length of 1.75 fm [13]. This deformation is considerably larger than that suggested by the microscopic calculation of Descouvemont *et al.* [41], so that we consider this calculation as an upper limit of the  ${}^8\text{Li}$  excitation effect on the elastic scattering. We calculated the ratio between the  ${}^8\text{Li}(0.98; 1^+)$  inelastic excitation cross section and the elastic one, in the whole angular range of the measurements, and the conclusion was that the effect of the  $1^+$  would be, at most, a few percent of the elastic one ( $<8\%$ ) at angles between  $40^\circ$  and  $80^\circ$ . The magnitude of this effect is smaller than the error bars of the measurements in this angular region. Thus, neither the CC effect nor the possible  $1^+$  inelastic contamination provides a reasonable explanation for the observed intermediate-angles rise of the elastic angular distributions. Our results are in agreement with those of Ref. [43], where probabilities below 2.5% for the  $1^+$  inelastic excitation have been reported. Thus, from now on, we will refer to the data as pure elastic scattering angular distributions.

In order to describe the intermediate rise within the optical model (OM), we supplemented the imaginary part of the DF potential with a surface (derivative) Woods-Saxon potential with adjustable parameters [17]. The fit was weakly sensitive to the normalization factor  $N_i$ , so the latter was conveniently kept fixed to  $N_i = 0.6$  (see the discussion in Sec. III D) whereas the depth ( $W_d$ ), the radius ( $r_d$ ), and the diffuseness ( $a_d$ ) were adjusted to reproduce the measured elastic data. This yielded the values  $W_d = 92$  MeV,  $r_d = 1.25$  fm, and  $a_d = 0.263$  fm. The results of these calculations are compared with the data in Fig. 3. The solid line is the OM fit with the surface derivative term included and the dashed line corresponds to the double-folding calculation with  $N_r = 1$  and  $N_i = 0.6$  without the surface derivative term.

The need for the inclusion of a surface imaginary potential is interpreted as an indication of strongly coupled direct reaction channels, which cannot be simply described by a mere scaling of the double-folding potential. Natural candidates are the channels responsible for the  ${}^7\text{Li}$  production since this is the main product observed in the spectra (cf. Fig. 1).

Since the removed neutron is not measured, several processes might in principle contribute to the  ${}^7\text{Li}$  production. These processes can be divided into two categories. On one hand, there are the so-called elastic breakup (EBU) channels, in which the projectile dissociates into  ${}^7\text{Li} + n$  whereas the

target remains in its ground state. On the other hand, there are those processes which involve some nonelastic interaction of the removed neutron with the target nucleus, which we denote globally as nonelastic breakup (NEB). The latter include the neutron stripping channels leading to bound states of the  ${}^{59}\text{Ni}$  nucleus, but also processes in which the neutron is transferred to states above the  ${}^{58}\text{Ni} + n$  threshold, such as the formation of a highly excited  ${}^{59}\text{Ni}$  compound nucleus. Since the present measurements are inclusive with respect to the removed neutron, these processes cannot be unambiguously disentangled with the data alone. To elucidate the nature of these processes and their effect on the elastic scattering cross section, in the next sections the measured elastic and inclusive breakup cross sections are compared with several model calculations. EBU and NEB channels are evaluated, respectively, with the CDCC and IAV methods. Finally, coupled-reaction-channels (CRC) calculations have been performed to investigate the influence of these channels on the elastic cross sections.

### B. CDCC calculations

For the CDCC calculations, the  ${}^8\text{Li}$  projectile was described as  ${}^7\text{Li}(\text{g.s.}) + n$ . For simplicity, the  ${}^7\text{Li}$  spin was ignored. The  ${}^8\text{Li}$  ground state was modeled as a valence neutron occupying a  $1p_{3/2}$  orbital and bound by  $S_n = 2.033$  MeV. The projectile breakup is described as inelastic excitations of this valence neutron to higher excited states lying in the continuum. These continuum states are discretized in energy bins for each angular momentum configuration, with  $\ell_{\text{max}} = 3$  and up to an excitation energy of  $\varepsilon_{\text{max}} = 9.3$  MeV. The CDCC calculations require also optical potentials for the  $n$ - ${}^{58}\text{Ni}$  and  ${}^7\text{Li} + {}^{58}\text{Ni}$  systems. For the former, the parametrization of Koning and Delaroche [44] was adopted. For the  ${}^7\text{Li} + {}^{58}\text{Ni}$  potential, the global parametrization of Cook [45] was initially considered, but the depths of the real and imaginary parts were further adjusted in order to best fit existing elastic scattering data for this system from Refs. [46–49] and constrained using dispersion relations, according to the analytic prescription of Ref. [50]. Following this work, the depth of the imaginary part was parametrized as

$$W(E) = W_0 \left[ \frac{1}{\pi} \arctan \left( \frac{E - E_0}{\Gamma} \right) + \frac{1}{2} \right], \quad (2)$$

which, using the subtracted dispersion relation, gives an energy-dependent correction term to the real part [50],

$$V(E) = -\frac{W_0}{\pi} \ln \left( \sqrt{1 + \left( \frac{E - E_0}{\Gamma} \right)^2} \right) + V_0. \quad (3)$$

The extracted values, evaluated at the present incident energies, are  $V_0 = 89.03$  MeV,  $r_0 = 1.286$  fm,  $a_0 = 0.853$  fm,  $W_0 = 27.221$  MeV,  $E_0 = 17.954$  MeV,  $\Gamma = 23.279$  MeV,  $r_l = 1.739$  fm,  $a_l = 0.809$  fm, and  $r_c = 1.3$  fm, and the radii were defined by  $R_x = r_x A_T^{1/3}$ .

The CDCC calculations were performed with the code FRESKO [51] and the  ${}^7\text{Li}$  angular and energy distributions were extracted from the calculated breakup scattering amplitudes using the formalism and codes developed in Ref. [52].

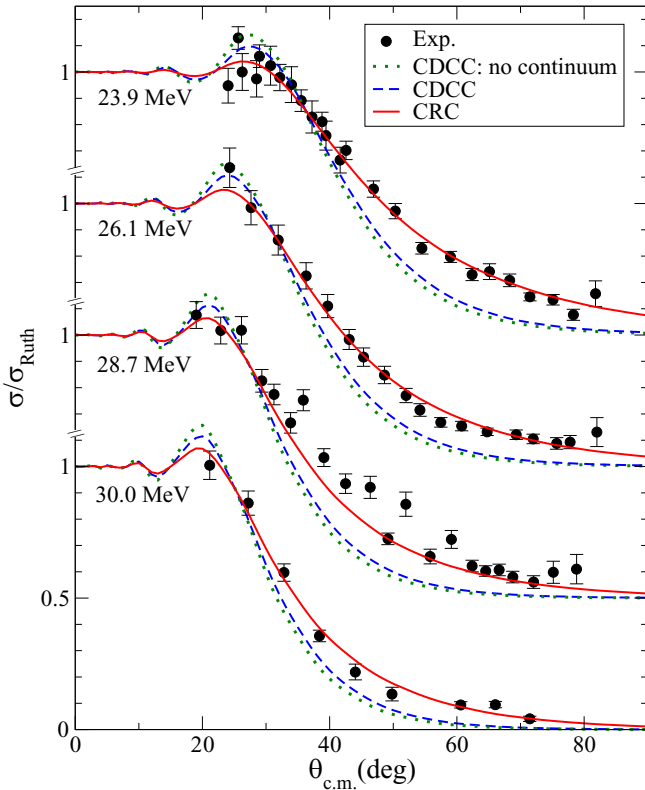


FIG. 6. The  $^8\text{Li} + ^{58}\text{Ni}$  elastic scattering angular distributions relative to Rutherford compared with CDCC (dashed lines) and CRC (solid lines) calculations at the four measured incident energies. The dotted lines are single-channel calculations obtained omitting the coupling to breakup channels in the CDCC calculations.

The results of these calculations are compared with the elastic data in Fig. 6 and with the  $^7\text{Li}$  angular and  $Q$  distributions in Figs. 4 and 5, respectively. To highlight the effect of the breakup channels on the elastic cross sections, single-channel calculations, in which the breakup channels are omitted, are also shown in Fig. 6 (dotted lines). The comparison of these single-channel calculations with the full CDCC results shows that the coupling to the breakup channels produces a reduction of the cross section at the rainbow peak, and a slight increase at intermediate angles. The effect is, however, too mild to explain satisfactorily the data at these scattering angles.

The arrows shown in Fig. 5, placed at  $Q = -2.03$  MeV, indicate the neutron separation threshold of  $^{59}\text{Ni}$  ( $S_n = 9$  MeV). Thus, the events with  $Q > -2.03$  MeV ( $Q < -2.03$  MeV) correspond to the population of bound (unbound) states of the  $^{59}\text{Ni}$  nucleus. It can be seen that about one-half of the  $^7\text{Li}$  yield is associated with the population of  $^{59}\text{Ni}$  bound states. By construction, this contribution is absent in the CDCC calculations. Moreover, even for  $Q$  values corresponding to breakup (i.e.,  $Q < -2.03$  MeV), the calculations largely underpredict the magnitude of the measured cross sections. These results clearly indicate that the elastic breakup mechanism is not the main contributor for the  $^7\text{Li}$  production and that the  $^7\text{Li}$  yields are mostly produced by one-neutron transfer channels

and other NEB mechanisms. These NEB contributions will be addressed in the next subsection with the aid of the IAV model.

### C. Nonelastic breakup contributions

According to the already discussed  $Q$ -value distributions, the range of excitation energies in the recoil system  $^{59}\text{Ni}$  is very broad, spanning from bound states up to well above the neutron separation threshold. Explicit inclusion of all these states would render the calculation very involved. Furthermore, the spin-parity assignment as well as their individual spectroscopic amplitudes are in many cases poorly known, particularly for states in the continuum. The inclusive breakup model of Ichimura, Austern, and Vincent (IAV) [53] provides a simpler and efficient alternative in which the distribution of populated states is encoded in a suitably chosen optical potential. The model is based on a participant-spectator picture of the reaction, which can be schematically represented as  $a + A \rightarrow b + B^*$ , where the projectile  $a$  dissociates into  $b + x$ , but only the fragment  $b$  (the spectator particle) is detected. The participant particle  $x$  corresponds to the unobserved particle (the neutron in our case). The residual nucleus  $B^*$  denotes any possible final state of the  $x + A$  system.

Below the  $x + A$  threshold ( $n + ^{58}\text{Ni}$  in our case), these states correspond to bound states of the  $B$  system ( $^{59}\text{Ni}$ ) and hence the underlying process is just a conventional one-neutron stripping [54,55]. Above the  $x + A$  threshold, the IAV method enables one to separate the inclusive cross section into EBU and NEB contributions, with the latter being associated with the absorption of the  $x + A$  optical potential. The mathematical details of the method can be found in the original work of IAV [53] as well in more recent applications [55–58].

In the present work, we adopt the distorted-wave Born approximation (DWBA) version of the IAV method, in which the entrance channel wave function is described as the product of the projectile ground-state wave function times a distorted wave describing the elastic scattering. For the former, we use the same neutron- $^7\text{Li}$  model employed in the CDCC calculations. The  $^8\text{Li} + ^{58}\text{Ni}$  distorted wave was generated with the optical model fit discussed in Sec. III A and shown in Fig. 3.

The comparison of these calculations with the  $^7\text{Li}$  angular and  $Q$ -value distributions is shown in Figs. 4 and 5, respectively. In addition to the NEB contribution, we display the total inclusive breakup contribution (EBU+NEB). The agreement with the data is very satisfactory at the four measured bombarding energies. As anticipated, NEB represents the dominant contribution of the  $^7\text{Li}$  yields. From the  $Q$ -value distribution, we see that the IAV calculations reproduce also the region corresponding to bound states. This result is less obvious, since the  $n + ^{58}\text{Ni}$  potential adopted in these calculations is not meant to describe the neutron negative energies. Part of this agreement might be due to the fact that the experimental energy resolution did not allow us to resolve specific bound states of the residual nucleus, and therefore only the gross features of the spectrum are observed.

From these results, it is also plausible that these strong NEB channels (including transfer to bound states) are also responsible for the deviation of the elastic scattering data

with respect to the double-folding calculations presented in Sec. III A. Being based in the DWBA approximation, the IAV model does not permit us to study the effect of NEB channels on the elastic data. To study such an effect, we have performed further calculations in which these couplings are included, approximately, within the CRC framework.

#### D. CRC calculations

The CRC method is a variational approach of the scattering process, in which the total wave function of the system is expanded in a set of internal states of two or more mass rearrangements [59,60]. The radial coefficients appearing in this expansion are obtained by solving a set of coupled integrodifferential equations. The method was originally devised to incorporate the effect of strong transfer channels in situations in which the first-order approximation (DWBA) is not valid. Included states are typically the ground state and a few low-lying excited states for the considered rearrangements. In the present case, we aim to use this method to describe the coupling of the elastic channels with the states of the  $^{59}\text{Ni}$  system. As the number of states in this energy range is expected to be enormous, we adopt an approximate procedure in which the physical states of the  $^{59}\text{Ni}$  system are replaced by a set of representative *doorway states*. For each angular momentum configuration ( $n\ell j$ ) above the Fermi level in  $^{58}\text{Ni}$ , we assume that the full single-particle strength can be described by a representative state, located at an excitation energy given by the centroid of the single-particle states belonging to this configuration, according to the analysis of the  $^{58}\text{Ni}(d, p)^{59}\text{Ni}$  reaction by Iwamoto *et al.* [61]. According to the results listed in Table 3 of Ref. [61], the relevant configurations are  $2p_{3/2}$ ,  $1f_{5/2}$ ,  $2p_{1/2}$ ,  $1g_{9/2}$ ,  $2d_{5/2}$ , and  $3s_{1/2}$ . It should be noted that the summed spectroscopic factors shown in that table, which were obtained from a DWBA analysis of the data, are in some cases significantly smaller than unity. The missing strength might correspond to unidentified levels but also to higher excited states lying in the continuum. In our calculations, we assign unit spectroscopic factor to all the above configurations, with the aim of accounting for this *missing strength*. We note also that, in addition to the aforementioned configurations, other higher single-particle configurations are also possible but, since they were not observed in the data of [61], we associate them with continuum states without significant bound states counterparts and, as such, they are described by a set of continuum bins. In this way, the calculation is meant to account, approximately, for the transfer of the neutron to both bound and unbound orbits of the  $^{59}\text{Ni}$  residual nucleus. Although one cannot make a one-by-one identification of the doorway states with the physical states of the system, completeness of the single-particle basis ensures that coupling with all relevant transfer channels is included.

We take into account the removal of the neutron from  $1p_{1/2}$  and  $1p_{3/2}$  configurations, leaving the  $^7\text{Li}$  in its first excited state. The required spectroscopic amplitudes for the  $^8\text{Li} \rightarrow ^7\text{Li} + n$  decomposition, considering  $^8\text{Li}$  in its g.s. or  $1^+$  excited state, have been taken from Ref. [62]. For  $^8\text{Li}(3^+) \rightarrow ^7\text{Li} + n$ , the required spectroscopic amplitude, corresponding

TABLE I. Total reaction and  $^7\text{Li}$  production cross sections for the  $^8\text{Li} + ^{58}\text{Ni}$  reaction at the incident energies measured in this work. NEB and EBU cross sections were obtained through IAV and CDCC calculations, respectively.

Energy (MeV)	$\sigma_{\text{reac}}^{\text{CRC}}$ (mb)	$\sigma_{\text{reac}}^{\text{OM-fit}}$ (mb)	$\sigma_{\text{bu}}^{\text{CRC}}$ (mb)	$\sigma_{\text{bu}}^{\text{NEB+EBU}}$ (mb)	$\sigma_{\text{bu}}^{\text{NEB}}$ (mb)
23.9	1354	1194	244	291	262
26.1	1484	1322	242	290	261
28.7	1606	1446	236	284	255
30.0	1657	1500	233	281	252

to the  $p_{3/2}$  configuration, was calculated following the same procedure adopted in Ref. [62], giving the value of 0.632.

As for the  $^8\text{Li}$  projectile, the CRC model space included, in addition to the  $^8\text{Li}$  ground state, the bound excited state ( $1^+$ ; 980.8 keV) and the narrow  $3^+$  resonance at  $E_x = 2.25$  MeV. Nuclear couplings between these three states were included by means of transition potentials generated by folding the M3Y nucleon-nucleon interaction with  $^8\text{Li}$  transition densities of Descouvemont *et al.* [41] and the target Hartree-Fock ground state density. Coulomb couplings were also included assuming a rotor model with matrix elements derived from the electric transition probability  $B(E2, 1^+ \rightarrow 2^+) = 1.6$  W.u. also computed in [41]. Transfer couplings from the  $^8\text{Li}$  ground state as well as from the considered excited states were included.

The CRC method requires also optical potentials for the entrance ( $^8\text{Li} + ^{58}\text{Ni}$ ) and exit ( $^7\text{Li} + ^{59}\text{Ni}^*$ ) channels. These are to be understood as *bare potentials*, which are meant to describe the interaction between the colliding partners in absence of the considered couplings. In practice, these bare potentials are adjusted so that the full CRC calculation reproduces the elastic scattering data. For the exit-channel optical potential, we adopted the parameters of the  $^7\text{Li} + ^{58}\text{Ni}$  potential discussed in Sec. III B. For the entrance channel, we found that a very good reproduction of the elastic data could be obtained by just removing the surface imaginary potential introduced in the OM analysis of Sec. III A and keeping the double-folding potential with scaling factors  $N_r = 1$  and  $N_i = 0.6$ . A reduction in the strength of the bare imaginary potential with respect to the optical model potential is expected since the couplings to the transfer channels are explicitly taken into account [63,64]. The same scaling factors were assumed for the transition potentials between the  $^8\text{Li}$  states.

The results of these calculations are compared with the elastic data in Fig. 6 and with the  $^7\text{Li}$  angular distributions in Fig. 4. Both observables are nicely explained by the calculations. Comparing the data with the full CRC calculation confirms the large influence of these channels on the elastic scattering, as was anticipated. In Table I we present the total reaction cross sections<sup>1</sup> obtained from the OM-fit (Fig. 3) and CRC calculations (Fig. 6), as well as the angle integrated

<sup>1</sup>The reaction cross section quoted here follows the definition of the FRESKO code [51].

transfer/breakup cross sections from CRC, IAV+CDCC, and IAV calculations (Fig. 4).

We end this section by noting that the conclusions of this work regarding the importance of the coupling to the one-neutron stripping channels are consistent with those found in Ref. [62] for the  ${}^8\text{Li} + {}^{208}\text{Pb}$  reaction.

#### IV. SUMMARY AND CONCLUSIONS

New experimental data of the  ${}^8\text{Li} + {}^{58}\text{Ni}$  elastic scattering and the  ${}^{58}\text{Ni}({}^8\text{Li}, {}^7\text{Li})$  reaction are presented at four incident energies above the Coulomb barrier. The  ${}^8\text{Li}$  beam was produced at the Radioactive Ion Beams in Brasil (RIBRAS) facility. A system of four silicon  $E$ - $\Delta E$  telescopes was used to detect the reaction products and identify the  ${}^8\text{Li}$  and  ${}^7\text{Li}$  isotopes with resolution sufficient to clearly separate the two isotopes. Angular and energy distributions were obtained for the elastic scattering and for the  ${}^7\text{Li}$  fragments. The  ${}^7\text{Li}$  angular distributions present a “bell shape” with a peak around the grazing angle, characteristic of a transfer process. The  ${}^7\text{Li}$  energy distributions indicate that the  ${}^{59}\text{Ni}$  recoil system is being populated in a broad excitation energy distribution below and above the neutron emission threshold, centered in the energy around the expected  $Q$  optimum for a neutron transfer reaction.

The elastic scattering angular distributions were first compared to the optical model using double-folding (DF) potentials. The optical model calculations with pure double-folding potential do not reproduce the angular distributions, overestimating the Fresnel peak and underestimating the cross sections for larger angles. An absorptive surface derivative term added to the DF potential was adjusted to reproduce the angular distributions indicating that the elastic scattering is largely influenced by strongly coupled direct reaction channels.

Continuum discretized coupled Channels calculations, considering the effect of the  ${}^8\text{Li}$  breakup into  $n + {}^7\text{Li}$ , reduce the elastic cross sections in the region of the rainbow peak, slightly increasing the cross section at larger angles, but not enough to explain the data. Moreover, these CDCC calculations largely underestimate the measured  ${}^7\text{Li}$  cross sections.

By contrast, inclusion of nonelastic breakup contributions, computed with the model of Ichimura, Austern, and Vincent, provides a very good agreement with the  ${}^7\text{Li}$  data for both angular and energy distributions. Since the IAV model does not allow one to describe the effect of the NEB on the elastic channel, a CRC analysis was performed considering the coupling between elastic scattering and the neutron transfer channels populating bound and unbound states of  ${}^{59}\text{Ni}$ . The agreement with both the elastic scattering and transfer angular distributions is remarkable, nicely reproducing the intermediate angles rise observed in the elastic distributions, revealing the strong influence of the neutron stripping channels on the  ${}^8\text{Li} + {}^{58}\text{Ni}$  scattering.

#### ACKNOWLEDGMENTS

This work has been partially supported by Conselho Nacional de Desenvolvimento Científico e Tecnológico, CNPq/MCTI (Brazil); by Fundação de Amparo à Pesquisa do Estado de São Paulo, FAPESP (Brazil), Contracts No. 2019/02759-0, No. 2019/07767-1, No. 2016/17612-7, and No. 2013/22100-7; by Coordenação de Aperfeiçoamento de Pessoal de Nível Superior, Brasil (CAPES), Finance Code 88887.355019/2019; and by Fundação de Amparo à Pesquisa do Estado do Rio de Janeiro, FAPERJ (Brazil). A.M.M. is supported by the Spanish Ministerio de Ciencia, Innovación y Universidades (including FEDER funds) under Project No. FIS2017-88410-P and by the European Union’s Horizon 2020 research and innovation program under Grant Agreement No. 654002.

- 
- [1] C. Beck, *Proceedings of the International Symposium on Exotic Nuclei, Exon-2018* (World Scientific, Singapore, 2018), pp. 9–16.
- [2] I. Tanihata, H. Hamagaki, O. Hashimoto, Y. Shida, N. Yoshikawa, K. Sugimoto, O. Yamakawa, T. Kobayashi, and N. Takahashi, *Phys. Rev. Lett.* **55**, 2676 (1985).
- [3] T. Kobayashi, O. Yamakawa, K. Omata, K. Sugimoto, T. Shimoda, N. Takahashi, and I. Tanihata, *Phys. Rev. Lett.* **60**, 2599 (1988).
- [4] N. A. Orr, N. Anantaraman, S. M. Austin, C. A. Bertulani, K. Hanold, J. H. Kelley, D. J. Morrissey, B. M. Sherrill, G. A. Souliotis, M. Thoennessen, J. S. Winfield, and J. A. Winger, *Phys. Rev. Lett.* **69**, 2050 (1992).
- [5] A. Lépine-Szily and R. Lichtenthäler, *Nucl. Phys. A* **787**, 94 (2007), in Proceedings of the Ninth International Conference on Nucleus-Nucleus Collisions.
- [6] F. D. Becchetti, W. Z. Liu, K. Ashktorab, J. F. Bajema, J. A. Brown, J. W. Jänecke, D. A. Roberts, J. J. Kolata, K. L. Lamkin, A. Morsad, R. J. Smith, X. J. Kong, and R. E. Warner, *Phys. Rev. C* **48**, 308 (1993).
- [7] S. Mukherjee, N. N. Deshmukh, V. Guimarães, J. Lubian, P. R. S. Gomes, A. Barioni, S. Appannababu, C. C. Lopes, E. N. Cardozo, K. C. C. Pires, R. Lichtenthäler, A. Lépine-Szily, D. S. Monteiro, J. M. B. Shorto, P. N. de Faria, E. Crema, V. Morcelle, M. C. Morais, and R. Pampa Condori, *Eur. Phys. J. A* **45**, 23 (2015).
- [8] A. Barioni, V. Guimarães, A. Lépine-Szily, R. Lichtenthäler, D. R. Mendes Jr., E. Crema, K. C. C. Pires, M. C. Morais, V. Morcelle, P. N. de Faria, R. P. Condori, A. M. Moro, D. S. Monteiro, J. M. B. Shorto, J. Lubian, and M. Assunção, *Phys. Rev. C* **80**, 034617 (2009).
- [9] V. Guimarães, R. Lichtenthäler, O. Camargo, A. Barioni, M. Assunção, J. J. Kolata, H. Amro, F. D. Becchetti, H. Jiang, E. F. Aguilera, D. Lizcano, E. Martínez-Quiroz, and H. Garcia, *Phys. Rev. C* **75**, 054602 (2007).
- [10] O. Camargo, V. Guimarães, R. Lichtenthäler, V. Scarduelli, J. J. Kolata, C. A. Bertulani, H. Amro, F. D. Becchetti, H. Jiang, E. F. Aguilera, D. Lizcano, E. Martínez-Quiroz, and H. Garcia, *Phys. Rev. C* **78**, 034605 (2008).
- [11] A. Pakou, D. Pierroutsakou, and M. Mazzocco, *Eur. Phys. J. A* **51**, 55 (2015).



- [12] A. Pakou, N. Keeley, D. Pierroutsakou, M. Mazzocco, L. Acosta, X. Aslanoglou, A. Boiano, C. Boiano, D. Carbone, M. Cavallaro, J. Grebosz, M. La Commara, C. Manea, G. Marquinez-Duran, I. Martel, C. Parascandolo, K. Rusek, A. M. Sánchez-Benítez, O. Sgouros, C. Signorini, F. Soramel *et al.*, *Eur. Phys. J. A* **51**, 90 (2015).
- [13] J. J. Kolata, V. Z. Goldberg, L. O. Lamm, M. G. Marino, C. J. O’Keeffe, G. Rogachev, E. F. Aguilera, H. García-Martínez, E. Martínez-Quiroz, P. Rosales, F. D. Becchetti, T. W. O’Donnell, D. A. Roberts, J. A. Brown, P. A. DeYoung, J. D. Hinnefeld, and S. A. Shaheen, *Phys. Rev. C* **65**, 054616 (2002).
- [14] T. Nakamura and Y. Kondo, *Clusters in Nuclei*, Lecture Notes in Physics Vol. 848 (Springer, Berlin, 2012), p. 67.
- [15] P. N. de Faria, R. Lichtenthäler, K. C. C. Pires, A. M. Moro, A. Lépine-Szily, V. Guimarães, D. R. Mendes Jr., A. Arazi, M. Rodríguez-Gallardo, A. Barioni, V. Morcelle, M. C. Morais, O. Camargo Jr., J. Alcántara Nuñez, and M. Assunção, *Phys. Rev. C* **81**, 044605 (2010).
- [16] P. N. de Faria, R. Lichtenthäler, K. C. C. Pires, A. M. Moro, A. Lépine-Szily, V. Guimarães, D. R. Mendes Jr., A. Arazi, A. Barioni, V. Morcelle, and M. C. Morais, *Phys. Rev. C* **82**, 034602 (2010).
- [17] P. Mohr, P. N. de Faria, R. Lichtenthäler, K. C. C. Pires, V. Guimarães, A. Lépine-Szily, D. R. Mendes, A. Arazi, A. Barioni, V. Morcelle, and M. C. Morais, *Phys. Rev. C* **82**, 044606 (2010).
- [18] K. C. C. Pires, R. Lichtenthäler, A. Lépine-Szily, V. Guimarães, P. N. de Faria, A. Barioni, D. R. Mendes Junior, V. Morcelle, R. Pampa Condori, M. C. Morais, J. C. Zamora, E. Crema, A. M. Moro, M. Rodríguez-Gallardo, M. Assunção, J. M. B. Shorto, and S. Mukherjee, *Phys. Rev. C* **83**, 064603 (2011).
- [19] K. C. C. Pires, R. Lichtenthäler, A. Lépine-Szily, and V. Morcelle, *Phys. Rev. C* **90**, 027605 (2014).
- [20] K. C. C. Pires, S. Appannababu, R. Lichtenthäler, and O. C. B. Santos, *Phys. Rev. C* **98**, 014614 (2018).
- [21] V. Morcelle, R. Lichtenthäler, R. Linares, M. C. Morais, V. Guimarães, A. Lépine-Szily, P. R. S. Gomes, J. Lubian, D. R. Mendes Junior, P. N. De Faria, A. Barioni, L. R. Gasques, J. M. B. Shorto, K. C. C. Pires, J. C. Zamora, R. P. Condori, V. Scarduelli, J. J. Kolata, H. Amro, F. D. Becchetti *et al.*, *Phys. Rev. C* **89**, 044611 (2014).
- [22] V. Morcelle, K. C. C. Pires, M. Rodríguez-Gallardo, R. Lichtenthäler, A. Lépine-Szily, V. Guimarães, P. N. Faria, D. R. Mendes Junior, A. M. Moro, L. R. Gasques, E. Leistenschneider, R. Pampa Condori, V. Scarduelli, M. C. Morais, A. Barioni, J. C. Zamora, and J. M. B. Shorto, *Phys. Lett. B* **732**, 228 (2014).
- [23] V. Morcelle, R. Lichtenthäler, A. Lépine-Szily, V. Guimarães, K. C. C. Pires, J. Lubian, D. R. Mendes Junior, P. N. de Faria, J. J. Kolata, F. D. Becchetti, H. Jiang, E. F. Aguilera, D. Lizcano, E. Martínez-Quiroz, and H. Garcia, *Phys. Rev. C* **95**, 014615 (2017).
- [24] E. Benjamim, A. Lépine-Szily, D. R. Mendes Jr., R. Lichtenthäler, V. Guimarães, P. R. S. Gomes, L. C. Chamon, M. S. Hussein, A. M. Moro, A. Arazi, I. Padron, J. Alcántara Nuñez, M. Assunção, A. Barioni, O. Camargo Jr., R. Z. Denke, P. N. de Faria, and K. C. C. Pires, *Phys. Lett. B* **647**, 30 (2007).
- [25] S. Appannababu, R. Lichtenthäler, M. A. G. Alvarez, M. Rodríguez-Gallardo, A. Lépine-Szily, K. C. C. Pires, O. C. B. Santos, U. U. Silva, P. N. de Faria, V. Guimarães, E. O. N. Zevallos, V. Scarduelli, M. Assunção, J. M. B. Shorto, A. Barioni, J. Alcántara-Núñez, and V. Morcelle, *Phys. Rev. C* **99**, 014601 (2019).
- [26] S. Santra, S. Kailas, V. V. Parkar, K. Ramachandran, V. Jha, A. Chatterjee, P. K. Rath, and A. Parihari, *Phys. Rev. C* **85**, 014612 (2012).
- [27] M. K. Pradhan, A. Mukherjee, S. Roy, P. Basu, A. Goswami, R. Kshetri, R. Palit, V. V. Parkar, M. Ray, M. Saha Sarkar, and S. Santra, *Phys. Rev. C* **88**, 064603 (2013).
- [28] K. J. Cook, I. P. Carter, E. C. Simpson, M. Dasgupta, D. J. Hinde, L. T. Bezzina, S. Kalkal, C. Sengupta, C. Simenel, B. M. A. Swinton-Bland, K. Vo-Phuoc, and E. Williams, *Phys. Rev. C* **97**, 021601(R) (2018).
- [29] K. J. Cook, E. C. Simpson, L. T. Bezzina, M. Dasgupta, D. J. Hinde, K. Banerjee, A. C. Berriman, and C. Sengupta, *Phys. Rev. Lett.* **122**, 102501 (2019).
- [30] E. Leistenschneider, A. Lépine-Szily, M. A. G. Alvarez, D. R. Mendes, R. Lichtenthäler, V. A. P. Aguiar, M. Assunção, R. P. Condori, U. U. da Silva, P. N. de Faria, N. Deshmukh, J. G. Duarte, L. R. Gasques, V. Guimarães, E. L. A. Macchione, M. C. Morais, V. Morcelle, K. C. C. Pires, V. B. Scarduelli, G. Scotton *et al.*, *Phys. Rev. C* **98**, 064601 (2018).
- [31] D. R. Mendes, A. Lépine-Szily, P. Descouvemont, R. Lichtenthäler, V. Guimarães, P. N. de Faria, A. Barioni, K. C. C. Pires, V. Morcelle, R. Pampa Condori, M. C. Morais, E. Leistenschneider, C. E. F. Lima, J. C. Zamora, J. A. Alcántara, V. Zagatto, M. Assunção, and J. M. B. Shorto, *Phys. Rev. C* **86**, 064321 (2012).
- [32] S. K. Das, T. Fukuda, Y. Mizoi, H. Ishiyama, H. Miyatake, Y. X. Watanabe, Y. Hirayama, S. C. Jeong, H. Ikezoe, M. Matsuda, K. Nishio, and T. Hashimoto, *Phys. Rev. C* **95**, 055805 (2017).
- [33] O. C. B. Santos, R. Lichtenthäler, K. C. C. Pires, A. M. Moro, U. Umbelino, E. O. N. Zevallos, M. Assunção, S. Appannababu, J. Alcántara-Núñez, A. L. de Lara, V. Scarduelli, V. Guimarães, A. Lépine-Szily, A. S. Serra, R. Linares, V. A. B. Zagatto, P. N. de Faria, V. Morcelle, M. C. Morais, A. Barioni *et al.*, *J. Phys.: Conf. Ser.* **1291**, 012030 (2019).
- [34] R. Lichtenthäler, A. Lépine-Szily, V. Guimarães, C. Perego, V. Placco, O. Camargo jr., R. Denke, P. N. de Faria, E. A. Benjamim, N. Added, G. F. Lima, M. S. Hussein, J. Kolata, and A. Arazi, *Eur. Phys. J. A* **25**, 733 (2005).
- [35] A. Lépine-Szily, R. Lichtenthäler, and V. Guimarães, *Eur. Phys. J. A* **50**, 128 (2014).
- [36] R. Lichtenthäler, M. A. G. Alvarez, A. Lépine-Szily, S. Appannababu, K. C. C. Pires, U. U. da Silva, V. Scarduelli, R. P. Condori, and N. Deshmukh, *Few Body Syst.* **57**, 157 (2016).
- [37] R. Lichtenthäler, O. C. B. Santos, A. Serra, U. Umbelino, K. C. C. Pires, J. R. B. Oliveira, A. Lépine-Szily, P. N. de Faria, and V. Morcelle, *Eur. Phys. J. A* **57**, 92 (2021).
- [38] R. Lichtenthäler (unpublished).
- [39] A. S. Freitas, L. Marques, X. X. Zhang, M. A. Luzio, P. Guillaumon, R. P. Condori, and R. Lichtenthäler, *Braz. J. Phys.* **46**, 120 (2016).
- [40] D. M. Brink, *Phys. Lett.* **40B**, 37 (1972).
- [41] P. Descouvemont and E. C. Pinilla, *Few-Body Syst.* **60**, 11 (2019).
- [42] B. A. Brown, *Phys. Rev. C* **58**, 220 (1998).
- [43] J. A. Brown, F. D. Becchetti, J. W. Jänecke, K. Ashktorab, D. A. Roberts, J. J. Kolata, R. J. Smith, K. Lamkin, and R. E. Warner, *Phys. Rev. Lett.* **66**, 2452 (1991).
- [44] A. J. Koning and J. P. Delaroche, *Nucl. Phys. A* **713**, 231 (2003).
- [45] J. Cook, *Nucl. Phys. A* **388**, 153 (1982).

- [46] P. Amador-Valenzuela, E. F. Aguilera, E. Martinez-Quiroz, D. Lizcano, and J. C. Morales-Rivera, *J. Phys.: Conf. Ser.* **876**, 012002 (2017).
- [47] D. Gupta, C. Samanta, R. Kanungo, M. K. Sharan, S. Kailas, A. Chatterjee, K. Mahata, and A. Shrivastava, *Nucl. Phys. A* **646**, 161 (1999).
- [48] C. W. Glover, R. I. Cutler, and K. W. Kemper, *Nucl. Phys. A* **341**, 137 (1980).
- [49] T. P. Morrison, G. D. Jones, L. P. Ekstrom, F. Kearns, P. R. G. Lornie, O. Mustafa, H. G. Price, D. N. Simister, P. J. Twin, and R. Wadsworth, *J. Phys. G: Nucl. Part. Phys.* **5**, 1751 (1979).
- [50] A. M. Moro and J. Gómez-Camacho, *Nucl. Phys. A* **648**, 141 (1999).
- [51] I. J. Thompson, *Comput. Phys. Rep.* **7**, 167 (1988).
- [52] J. A. Tostevin, F. M. Nunes, and I. J. Thompson, *Phys. Rev. C* **63**, 024617 (2001).
- [53] M. Ichimura, N. Austern, and C. M. Vincent, *Phys. Rev. C* **32**, 431 (1985).
- [54] T. Udagawa, Y. J. Lee, and T. Tamura, *Phys. Lett.* **196B**, 291 (1987).
- [55] G. Potel, G. Perdikakis, B. V. Carlson, M. C. Atkinson, W. H. Dickhoff, J. E. Escher, M. S. Hussein, J. Lei, W. Li, A. O. Macchiavelli, A. M. Moro, F. M. Nunes, S. D. Pain, and J. Rotureau, *Eur. Phys. J. A* **53**, 178 (2017).
- [56] J. Lei and A. M. Moro, *Phys. Rev. C* **92**, 044616 (2015).
- [57] G. Potel, F. M. Nunes, and I. J. Thompson, *Phys. Rev. C* **92**, 034611 (2015).
- [58] B. V. Carlson, R. Capote, and M. Sin, *Few-Body Syst.* **57**, 307 (2016).
- [59] G. Satchler, *Direct Nuclear Reactions*, International Series of Monographs on Physics (Clarendon, Oxford, 1983).
- [60] J. G. Camacho and A. M. Moro, *The Euroschool on Exotic Beams* (Springer, Berlin, 2014), Vol. IV, pp. 39–66.
- [61] O. Iwamoto, A. Nohtomi, Y. Uozumi, T. Sakae, M. Matoba, M. Nakano, T. Maki, and N. Koori, *Nucl. Phys. A* **576**, 387 (1994).
- [62] A. M. Moro, R. Crespo, H. Garcia-Martinez, E. F. Aguilera, E. Martinez-Quiroz, J. Gomez-Camacho, and F. M. Nunes, *Phys. Rev. C* **68**, 034614 (2003).
- [63] D. Pereira, J. Lubian, J. R. B. Oliveira, D. P. de Sousa, and L. C. Chamon, *Phys. Lett. B* **670**, 330 (2009).
- [64] U. Umbelino, K. C. C. Pires, R. Lichtenthäler, V. Scarduelli, G. A. Scotton, A. Lépine-Szily, V. Guimarães, J. Lubian, B. Paes, J. L. Ferreira, M. A. G. Alvarez, J. M. B. Shorto, S. Appannababu, M. Assunção, R. P. Condori, and V. Morcelle, *Phys. Rev. C* **99**, 064617 (2019).